Chapter 6

Mixed Ligand Transition Metal Complexes of Curcumin: Synthesis, DNA Binding and *in vitro* Antitumor Activity.

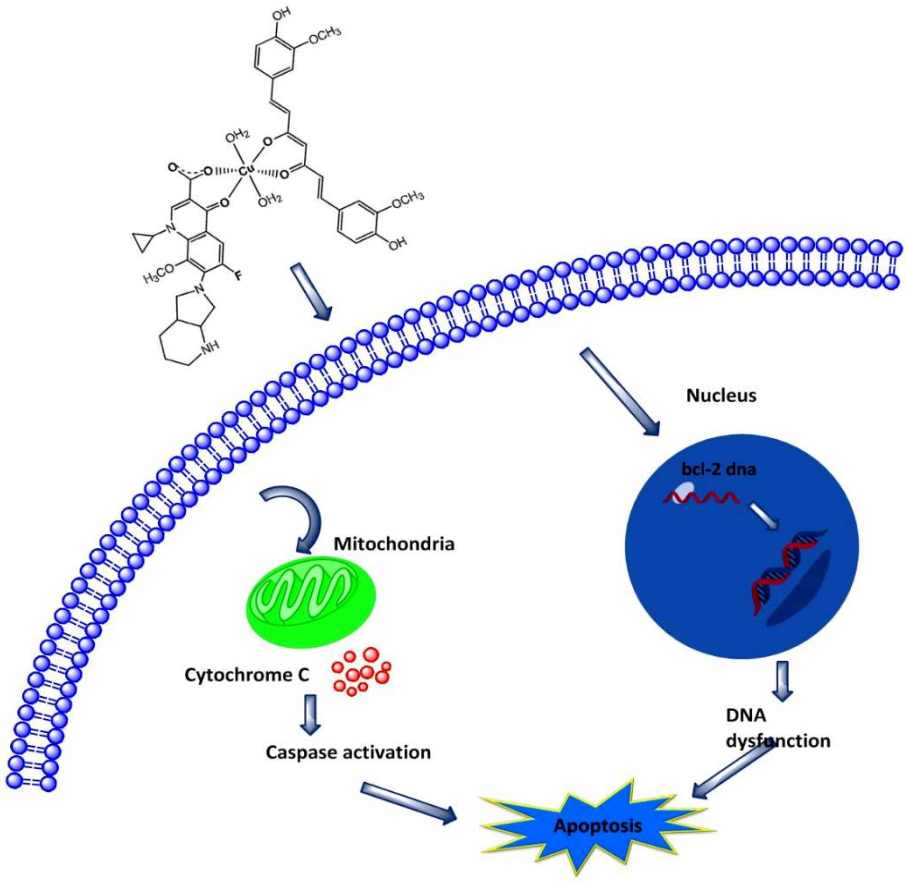

6.1 Introduction

"From kitchen to clinic" or "Curry against Alzheimer" – these are only two of the recent sensational headlines associated with the various health benefits of curcumin. Curcumin 1(=1,7-bis-(4-hydroxy-3-methoxyphenyl)-1,6-heptadiene-3,5-dione) is a component of the Indian spice turmeric, manufactured from the rhizome of the perennial herb *Curcuma longa* that is widely cultivated in tropical countries in South and South East Asia, especially in China and India [1].

Curcuma longa belongs to the Zingiberaceae (ginger) family. Curcumin (=CurcH) is the major component of three curcuminoids that give turmeric its characteristic yellow color and is used as a food colorant, flavoring and additive. The minor curcuminoid components are demethoxycurcumin (=DMCurcH) and bis-demethoxycurcumin (=BDMCurcH) in which one or both –OMe functionalities at the outer phenol rings are removed [2]. Besides its widespread use as food flavor and colorant, turmeric has been used in traditional Chinese and Ayurvedic medicine for around 4000 years. It was found that incidents of Alzheimer's disease among elderly people of age 70–79 in rural India, who eat curry dishes on a daily basis, is about 4.4 times lower than that of Americans of the same age [2]. Over the past few decades, numerous studies have explored the medicinal properties of turmeric and curcumin, including antitumoral, antimicrobial, anti-inflammatory, antioxidant, antihepatotoxic, antihyperlipidemic, antiviral, and anti-

Alzheimer's disease effects. In fact, turmeric has even been termed the "multi-antispice" in herbal medicine, and curcumin has been referred to as"curecumin" [3,4].

The anticancer properties include suppression of cellular transformation, prevention of cancer cell proliferation, and suppression of carcinogenic effects [5]. Curcumin compounds alone or in combination with other anticancer drugs have been reported to inhibit the clonogenicity of cancer cells and induce anti-proliferative and apoptotic effects on drug resistant cancer cells as well as reverse their chemoresistance. Thereby they improve the cytotoxic effects induced by diverse chemotherapeutic drugs on these immature cancer cells. These beneficial health effects of curcumin are all well documented in the current literature.

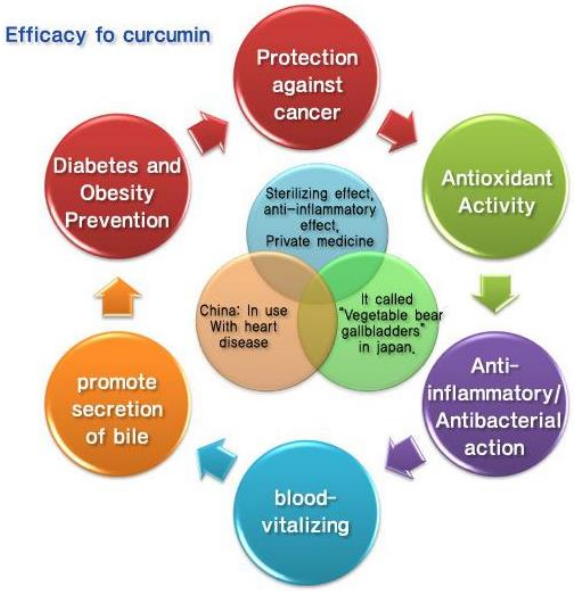

For example, in 2013 the journal "Current Pharmaceutical Design" published a special issue entitled "Recent Progress and Novel Insights in Curcumin Research – From Chemistry to Clinical Use". Clinical studies in humans showed that curcumin is generally safe even at high daily doses of up to 12 grams with only few side-effects [4].

A severe problem encountered in clinical trials involving curcumin is its poor bioavailability, leading to low levels in plasma and tissues. The insolubility of curcumin in water, poor absorption, rapid metabolism and systemic elimination has been shown to be the main factors limiting its bioavailability. As a result, numerous studies have been directed to increasing curcumin bioavailability, including the use of compounds which facilitates their absorption (e.g. piperidine/piperine), the encapsulation of curcumin in the cavities of cyclodextrins, or the use of nanoparticles [5] and ceramic particles [6]. A highly promising and innovative approach to deal with

the bioavailability issue and to achieve even more diverse potential health benefits is the use of metal curcumin complexes [7]. Curcumin and the curcuminoids are rare examples of naturally occurring β-diketone ligands. As such, they should be ideally suited to act as chelating ligands toward a variety of metals and to form stable complexes. The past 10 years have witnessed a dramatic increase in studies directed to the synthesis, characterization and biological investigation of metal curcumin complexes [8]. The three most exciting areas appear to be selective cytotoxicity and anticancer activity, anti-Alzheimer's activity, and antioxidative/neuroprotective effects. However, highly promising results with metal curcumin complexes have also been reported in the fields of antimicrobial/ antifungal activity, anti-viral/anti-HIV activity and biological imaging/radioimaging.

Excess of evidence indicated that curcumin metal complexes contribute to the inhibition of tumor formation, promotion, progression, and dissemination of tumor in many animal models although the mechanism of its anti-proliferative and apoptotic effects is still an enigma [8]. The clinical application of curcumin is limited due to its hydrolytic instability under physiological conditions. The degradation of curcumin could be arrested on binding to a metal ion. These emerging results encouraged us to synthesise and explore the mechanism of antiproliferative activitiy of curcumin metal complexes.

We have designed and prepared transition metal complexes (Cu^{2+},VO^{2+},Zn^{2+}) of curcumin with moxifloxacin (MFL) as ancillary ligand and investigated the interaction between curcumin metal complexes and DNA via electronic absorption spectroscopy, fluorescence spectroscopy and viscosity measurements. Curcumin upon binding to metal ion is expected to be stable in the biological pH. The dye being a photosensitizer, its emission property could be used for cellular imaging by fluorescence microscopy. The MFL moiety with its lipophilic nature is expected to enhance the cellular uptake of the designed complexes. The complexes were tested for their toxicity in A549 cancer cell lines and mechanism by which these metal

complexes induces apoptotic effects and whether an anti-apoptotic protein plays any role in curcumin metal complexes induced apoptosis were investigated.

6.2 General synthesis of complexes

Complexes **C1–C3** were prepared by a general synthetic procedure in which methanolic solution of metal salt (1.5 mmol) was added to a methanolic solution of MFL (1.5 mmol). The resulting solution was refluxed for 1 h followed by addition of the curcumin (1.5 mmol). The reaction mixture was cooled and stirred for 2 h at room temperature to get a solid precipitate. The solid was isolated, washed with methanol and dried in vacuum over P_4O_{10}.

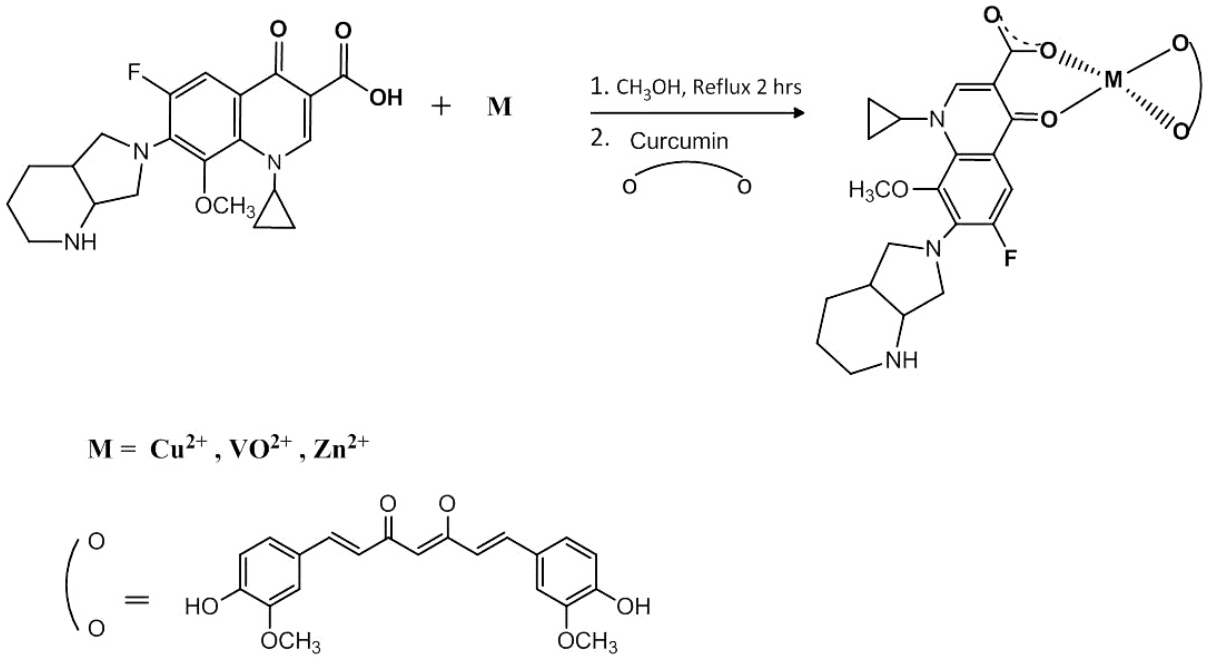

Scheme 6.1

6.3 Physicochemical data of the synthesized complexes

All the complexes were synthesized by the method described in section 6.2.

A. [Cu(MFL) (Cur)] (**C1**)

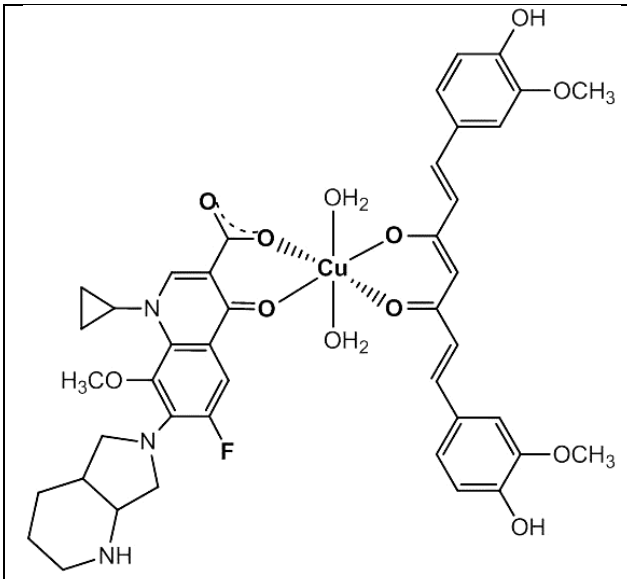	Yield: 69% Molecular weight: 868.38 g/mol Molecular formula: $C_{42}H_{47}CuFN_3O_{12}$ Calc. (%): C,58.09; H, 5.46; N, 4.84; Cu, 7.32 Found (%): C, 58.10; H, 5.48; N, 4.86; Cu, 7.4 λ_{max} :289, 456 nm. ESI-MS [MeOH, *m/z*]: 866.2 [M-2] IR: 1451 (COO_{asym}), 1348(COO_{sym}), 1682 $(C=O)_{py}$

B. [VO (MFL) (Cur)] (**C2**)

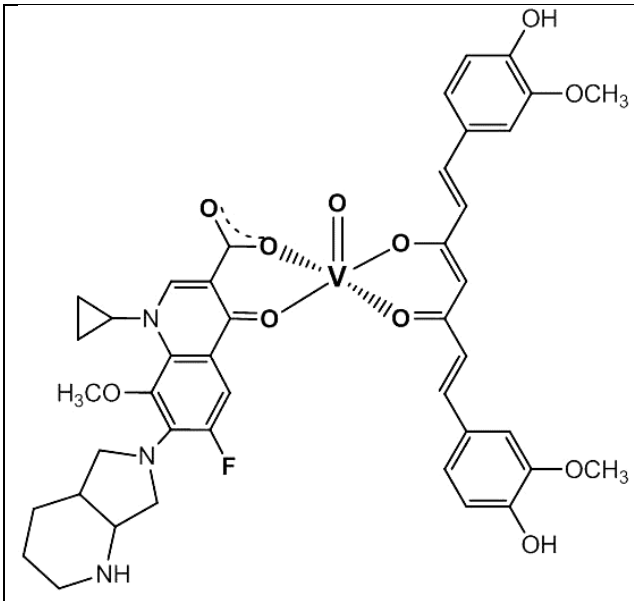	Yield: 73% Molecular weight: 835.74 g/mol Molecular formula: $C_{42}H_{43}VFN_3O_{11}$ Calc. (%): C, 60.36; H, 5.19; N, 5.03; V, 6.10 Found (%): C, 61.21; H, 5.20; N, 5.05; V, 6.18 λ_{max} :290, 460 nm. ESI-MS [MeOH, *m/z*]: 834.2[M-1] IR: 1456(COO_{asym}), 1345(COO_{sym}), 1688$(C=O)_{py}$

C. [Zn(MFL) (Cur)] (**C3**)

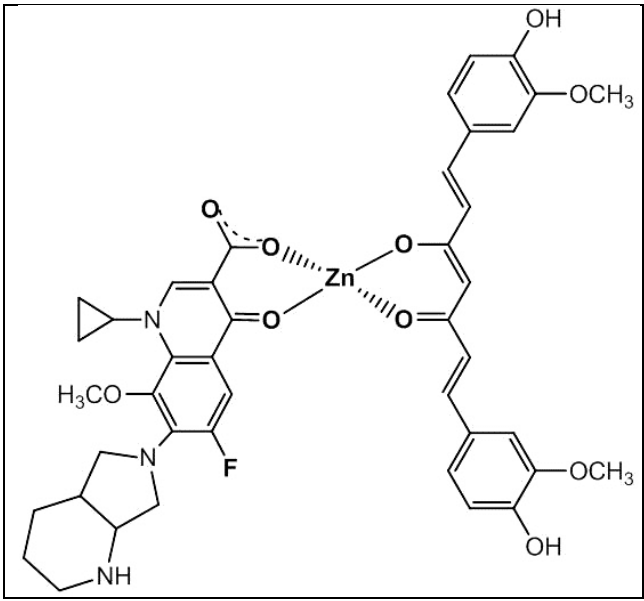

Yield:70%
Molecular weight: 834.18 g/mol
Molecular formula: $C_{42}H_{43}ZnFN_3O_{11}$
Calc. (%): C, 60.47; H, 5.20; N, 5.04; Zn, 7.84
Found (%): C, 60.41; H, 5.19; N, 5.05; Zn, 7.82
λ_{max} :287, 452 nm.
ESI-MS [MeOH, *m/z*]: 834.1[M^+]
IR: 1458 (COO_{asym}), 1348(COO_{sym}), 1680$(C=O)_{py}$

6.4 Results and discussions

6.4.1 Synthesis and general properties

The metal complexes (**C1-C3**) were prepared in high yields (~70%) by the reaction of MFL and curcumin (cur) with the metal salts in the ratio 1:1:1. The complexes were characterized by various spectroscopic and analytical techniques.

The IR spectra of the free ligands and their metal complexes were recorded in 4000-400 cm^{-1} range. The spectra of metal complexes were interpreted by comparing with the free ligands, in order to characterise their structures and mode of coordination of the ligands with the metal ions. The diagnostics infrared spectral data of free curcumin ligand and their complexes are listed in Table 6.1. The IR spectrum of cur showed a weak broad band at 3200 cm^{-1} which was assigned to enolic –OH group of free curcumin moiety. Disappearance of this band in all the complexes indicated the deprotonation of the enolic group upon coordination. The υ(CO) band at 1628 cm^{-1}, is shifted to lower energy (1593-1597 cm^{-1}) on complexation with the metal ions, indicating that the carbonyl group of the cur in the enol form is coordinated to the metal ions. Similarly the lower energy shifts in the pyridone carbonyl $\nu(CO)_{MFL}$ and

carboxylate $\nu(COO)_{MFL}$ stretching frequencies of moxifloxacin in complexes was due to binding of these groups with the metal ions. All the important stretching values have been tabulated in Table 6.1.

Table 6.1: Characteristic IR bands (4000–400 cm^{-1}) of complexes **C1-C3**.

Compounds	IR stretching values (cm^{-1})						
		Curcumin		C=CH	MFL		
	υ(C=O) keto	δ(CO) enol	δ(CO) phenol		υ(C=O)p	υCOO assym	υCOO sym
MFL	-	-	-	-	1708	1624 (Free COOH)	
Cur	1628	1427	1277	812	-	-	-
C1	1597	1408	1273	821	1682	1451	1347
C2	1593	1404	1280	828	1688	1456	1345
C3	1596	1406	1279	829	1680	1458	1348

The ESI-MS spectra of **C1** (Fig 6.1), **C2** and **C3** showed molecular ion peaks at m/z values equivalent to their molecular weights. The m/z values of all the complexes are in well agreement with the proposed composition (Section 6.3). Furthermore the composition and purity of the complexes have been confirmed by their C, H, N elemental analysis.

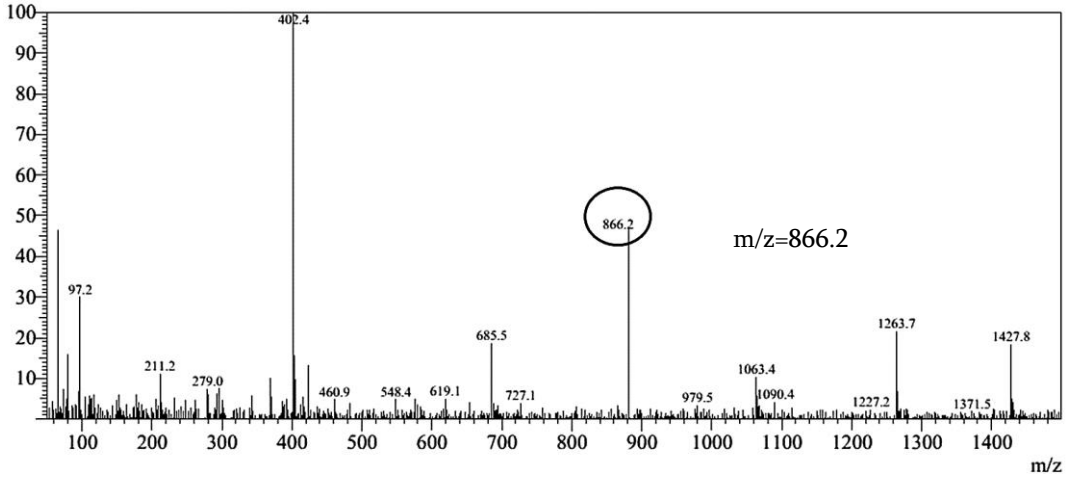

Fig 6.1: ESI-MS spectra of **C1**

The electronic absorption spectra of the ligands and complexes **C1-C3** in methanol were recorded in the region 200-900nm. The electronic spectrum of free Cur displayed intense absorption bands at 430 nm ascribed to n-π* transitions, which is observed to be red shifted in the spectra of **C1-C3** (Fig. 6.3, Table 6.2). Free MFL showed characteristic band at 286nm assigned to π-π* transitions; which is slightly shifted in the range of 287-290 nm on coordination with the metal ions.

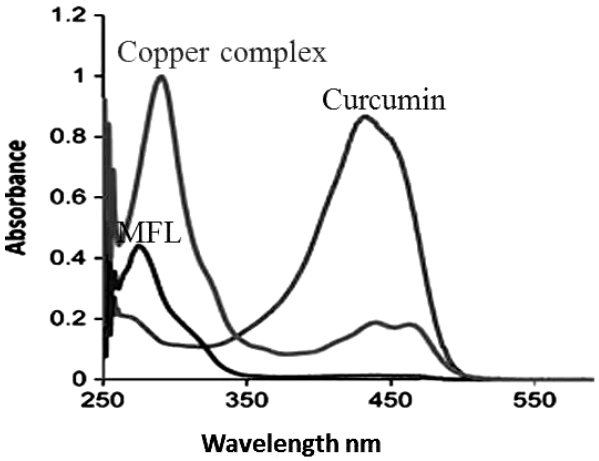

Fig 6.3: Electronic spectra of MFL, Cur and **C1** in methanol.

Table 6.2: Electronic spectral data of **C1-C3**.

	π-π* transitions nm	**n-π* transitions nm**
MFL	286	
Cur	-	430
C1	289	456
C2	290	460
C3	287	452

The EPR spectra of copper and vanadyl complexes exhibited hyperfine splitting (Fig.6.4) and the corresponding $g_{\|}$, $g_{\perp}$ and $A_{\|}$ values are tabulated in Table 3. The analysis of low temperature X-band EPR spectra of **C1** at 10 K in dmso is typical for a mononuclear Cu^{2+}complex in a distorted octahedral geometry (Fig. 6.4(a)). A nuclear hyperfine splitting of $g_{\|}$ signal due to copper nuclei in parallel orientation was observed whereas no observable splitting of $g_{\perp}$ signal was seen. The spectrum is typical of axially symmetric Cu(II) having one unpaired electron in $d_{x^2-y^2}$ orbital of the metal ion(Fig. 6.4(a)). The value of exchange interaction term G>4 (Table 3) indicates absence of Cu-Cu interaction, thus supporting proposed monomeric structure.

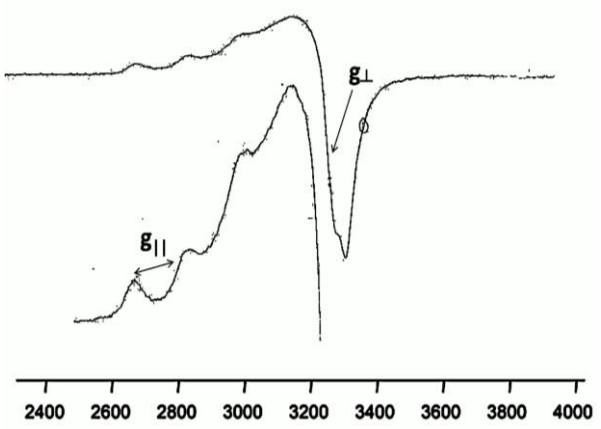

Fig 6.4 (a): ESR spectra of **C1** in DMSO. EPR conditions: Temperature, 10K; microwave power, 5.0 mW; Modulation amplitude, 1G; microwave frequency, 9.1 Ghz.

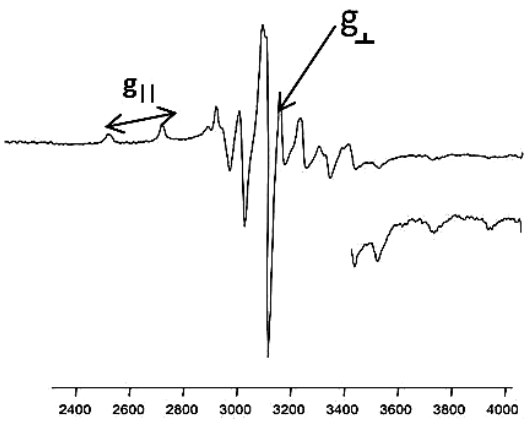

Fig 6.4 (b): ESR spectra of **C2** in DMSO. EPR conditions: Temperature, 10K; microwave power, 5.0 mW; Modulation amplitude, 1G; microwave frequency, 9.1 Ghz.

Table 6.3: X-band ESR parameters of **C1** and **C2.**

Compound	$g_{\|\|}$	$g^{\perp}$	$g_{average}$	$A_{\|\|}$	$A^{\perp}$	G
C1	2.12	2.05	2.12	170×10^{-4}	76×10^{-4}	4.19
C2	1.86	2.00	2.07	190×10^{-4}	36×10^{-4}	6.2

The EPR spectrum of **C2** exhibited a hyperfine eight-line pattern, characteristic of an unpaired electron being coupled with a vanadium nuclear spin (I=7/2). The spectrum displayed well-resolved hyperfine lines and the signal parameters for the complex are given in table 6.3. The parameters $g_{\|}$ and $A_{\|}$ have been estimated by considering the position of the outermost lines and the experimentally deduced pair of their values supported an O_4 basal plane at the equatorial sites of the VO^{2+}moiety.

6.4.2 Cytotoxicity studies

6.4.2.1 MTT Assay

Cytotoxicity tests were performed using the MTT assay wherein A549 cells were treated with the complexes **C1-C3** at varying concentrations (10–100μg/ml) for 12 h. All the complexes inhibited the growth of lung cancer cells significantly and recorded 50–85% higher cytotoxicity compared to the either MFL or curcumin with **C1** exhibiting promising growth inhibitory effect (Fig 6.5,Table 6.4).

Table 6.4: IC_{50} values of **C1-C3** obtained from MTT assay on A549 cells.

Compounds	MFL	Cur	C1	C2	C3
IC_{50} μg/ml	52.5	38.2	23.2	27.4	31.0

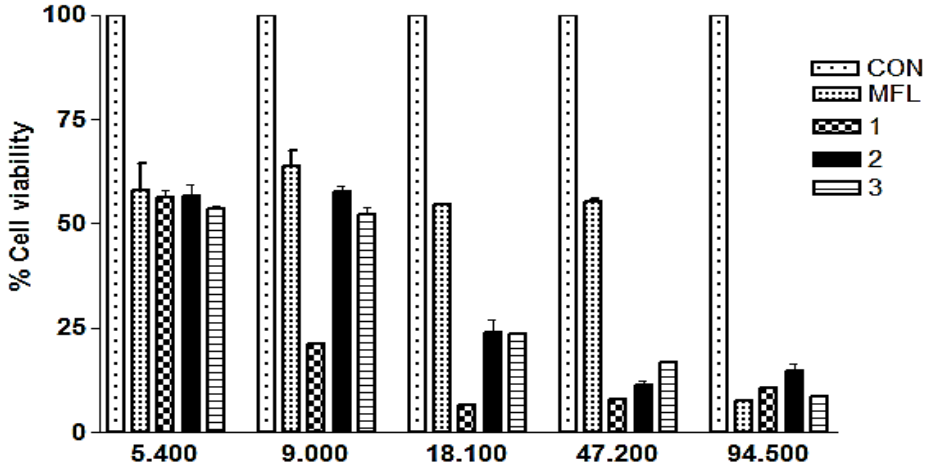

Fig 6.5: % cell viability in presence of **C1-C3** for A549 human lung cancer cell lines. Each point is the mean ± standard error obtained from three independent experiments.

6.4.2.2 Cellular uptake studies:

The cell-membrane is the structure that protects living cells from the surrounding environment, only allowing the movement of compounds generally with small molecular size across this barrier into the cell. As the complexes are stable in aqueous

solution and luminescent with an increase in luminescence intensity upon binding with DNA, the cellular uptake of C1 inside A549 cells was studied by using confocal microscopy [9]. Cellular uptake of **C1** inside A549 cells, was studied by confocal microscopy. Imaging was studied out by staining with Dapi (nuclear stain) to identify localization of the complex and any nuclear disintegration. Cells not treated with C1 exhibited negligible luminescence. Whereas, on treatment with **C1**, bright green fluorescence in the cytoplasm of the cells was observed (Fig. 6.6), indicating the uptake of **C1** by the cells. Fluorescence intensity was found to increase with time indicating increased internalization of the complexes. Similar results were obtained for **C1** and **C2**. Result reveal that **C1-C3** can enter and accumulate in cytosol of A549 cells.

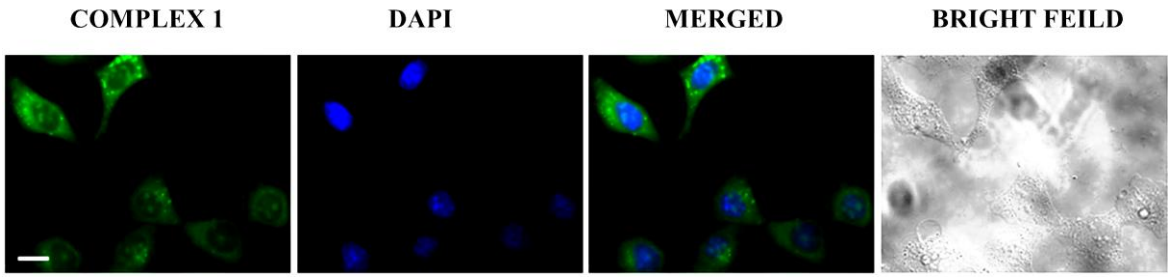

Fig 6.6 : Confocal microscopic images of A549 cells treated with **C1** and Dapi (A) green emission of **C1** (B) nucleus stained with Dapi(C) Merged image of A and B (D) Bright field image of A549 cells treated with **C1** for 6 hr at 37°C.

6.4.2.3 Cell cycle arrest analysis

Since the induction of apoptosis may be mediated through cell cycle arrest, we have examined the effect of **C1-C3** on cell cycle perturbations. The effect of **C1-C3** on cell cycle was evaluated using FACS analysis in propidium iodide (PI) stained A549cells. After 16 h treatment with **C1** (23.2 μg/ml), **C2** (27.4 μg/ml) and **C3** (31.0 μg/ml), cell population in the Sub G0/G1 phase increased from 38.2% (control) to 79.3% , 76.9% and 72.4 % respectively. The increase of cell population at Sub G0/G1 phase was accompanied by decrease in the cell population in G0/G1 phase of the cell cycle indicating arrest of cell cycle progression (Fig. 6.7(a) & 6.7(b)).

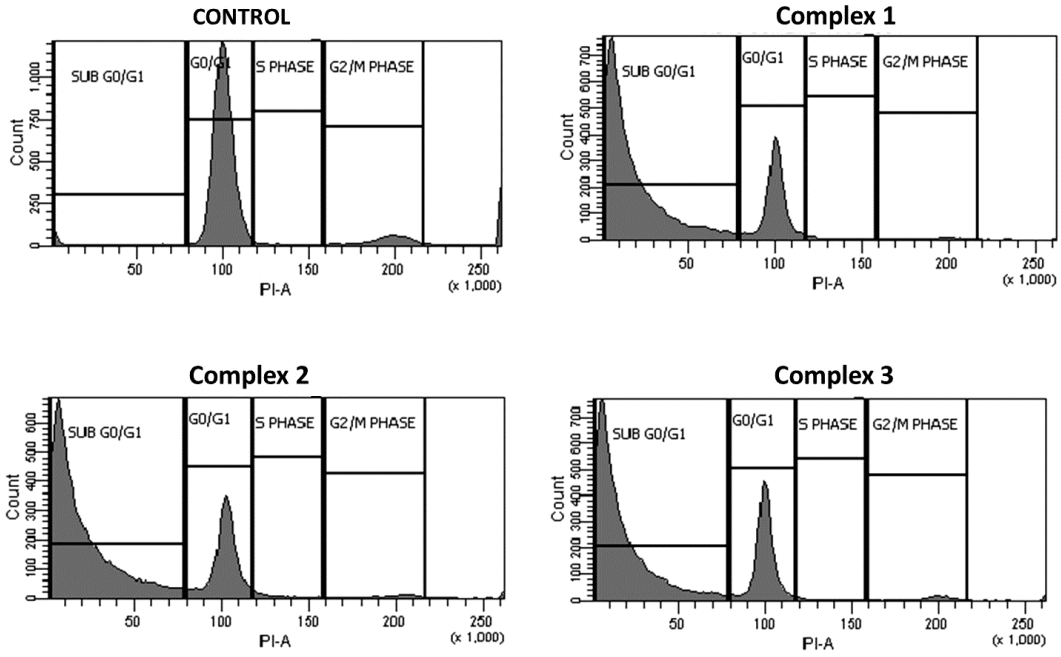

Fig 6.7 (a): Effects of **C1-C3** on A549 tumor cells after 16 h, distribution among cell cycle phases.

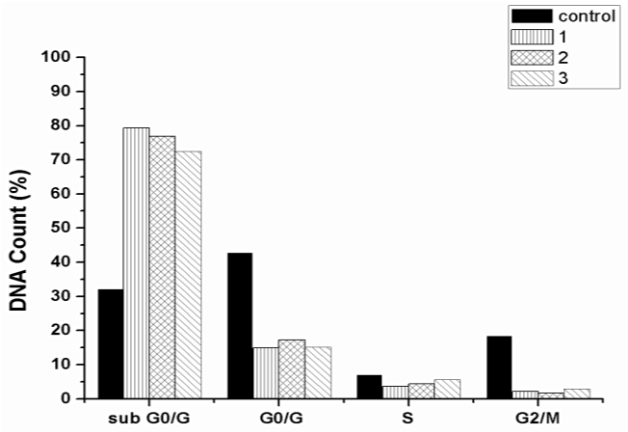

Fig 6.7 (b): Cell cycle distribution on exposure of A549cells to complexes **C1-C3** (IC_{50}).

6.4.2.4 Apoptotic inducing activity: FACS Analysis

The apoptotic studies were carried out using flow cytometer and the AnnexinV reagent. In the early stages of apoptosis, the cell membrane can expose phosphatidylserine (PS) which is annexin V-positive [10]. The measurement of annexin V binding to the cell surface as an indicator for apoptosis was performed along with a dye exclusion test, to establish the integrity of the cell membrane. The percentage of apoptotic cells and changes in DNA content distribution in A549 cells

treated with **C1-C3** is detected by analyzing with PI, and Annexin V binding using flow cytometry. Viable cells did not bind to annexin V or PI ($FITC^{-}P^{-}$;lower left quadrant D3), early apoptotic cells bound to annexin V but excluded PI ($FITC^{+}$ PI^{-};lower right quadrant D4) and necrotic or late apoptotic cells were both annexin V and PI positive ($FITC^{+}$ PI^{+}; upper right quadrant D1). The upper left quadrant D2 contains dead cells ($FITC^{-}$ PI^{+}). The percentage of apoptotic cells in A549 cells treated by **C1-C3** for 16 h increased in late apoptotic quadrant (upper right quadrant D1). The results are depicted in Fig. 6.8(a) and 6.8(b). The order of the percentage of late apoptotic cells in A549 cells treated with complexes **C1–C3** (IC_{50}) for 16 h is as follows: **C3** < **C2**< **C1** (**C1**–41.2 %, **C2**–33.3 %, **C3**–30.1%). These results indicated that the complexes can induce apoptosis of A549 cell line.

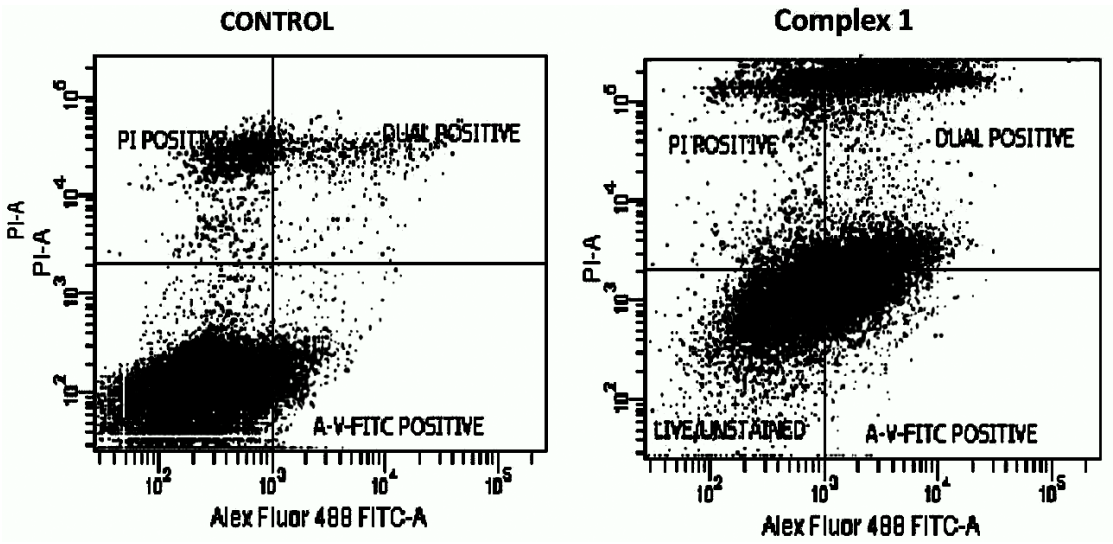

Fig 6.8 (a): Annexin V staining shows induction of apoptosis of A549 cells treated with **1** 16 h. The percent of apoptotic cells were detected by analysing Annexin V and PI binding with the help of flow cytometry. Viable cells did not bind to Annexin V or PI (lower left quadrant D3), early apoptotic cells bound to Annexin V but excluded PI (lower right quadrant D4), and late apoptotic cells were both annexin V- and PI-positive (upper right quadrant D2), the upper left quadrant D1 contains the nuclear debris or dead cell.

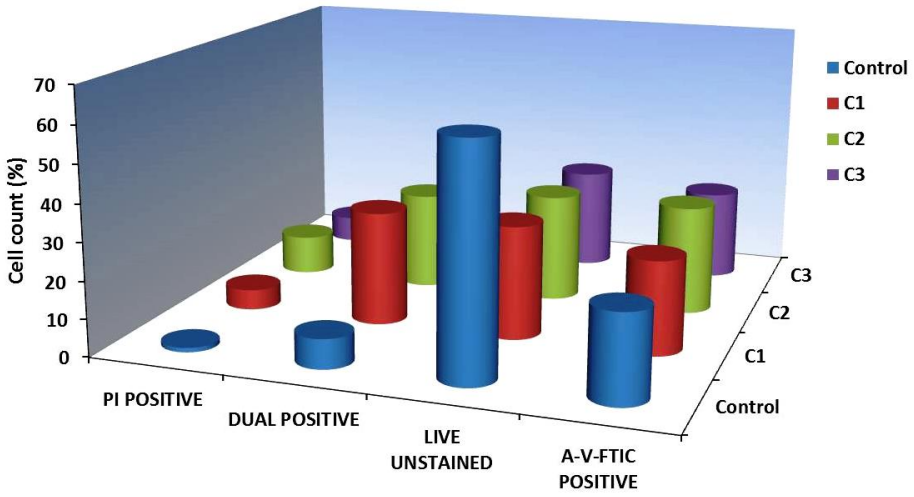

Fig 6.8 (b): Graphical representation of flow-cytometric analysis of apoptosis induced in A549 cells on treatment with **C1-C3** for 16h. Data is represented in the form of percentage of apoptotic population.

6.4.2.5 Measurement of Oxidative stress

ROS include the superoxide radical ($O2^{-\cdot}$), hydrogen peroxide (H_2O_2), and the hydroxyl radical ($OH^{\cdot}$). Oxidative stress generated by an imbalance between ROS and antioxidants contributes to the pathogenesis of cancer and other diseases [11]. ROS are not only cytotoxic by-products that trigger cell death through oxidative damage, but can also act as signaling molecules targeting specific components of metabolic and signal transduction pathways [11].

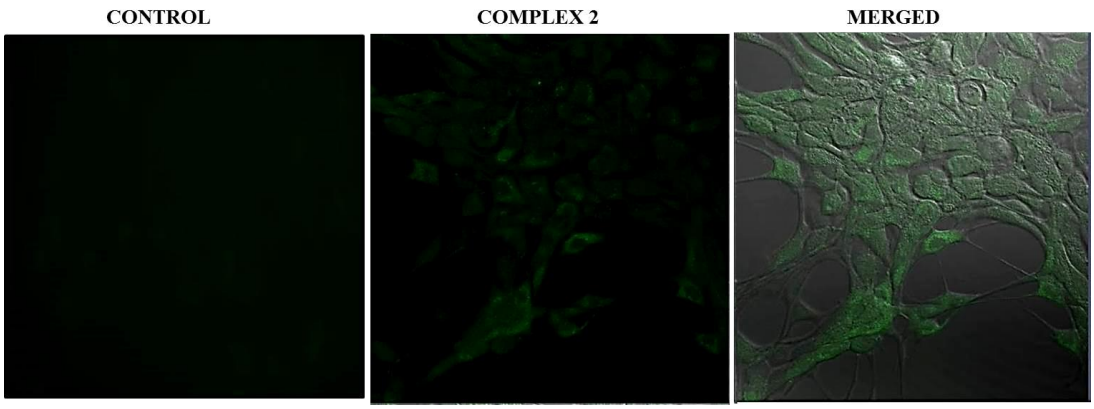

Fig 6.9: Microphotographs of A549 cells stained with DCFDA and observed under confocal microscope: (C) A549 cell without treatment; (1) in the presence of **C2**; incubated at 37˚C and 5% CO_2 for 16h.

To study whether the cell death induced by **C1-C3** is due to ROS generation and enhanced ROS levels, A549 cells were treated with **C1-C3** (IC_{50}) for 16 h. As shown in Fig. 6.9, A549 cells treated with **C2** and stained with DCFDA, a significant increase in the fluorescence intensity of dichlorofluorescein compared with that of the control was observed. This indicates that **C2** generated ROS there by enhancing the level of intracellular ROS (Section 3.4.6.5, chapter 3). Similar results were obtained for **C1** & **C3** complexes.

6.4.2.6 Assessment of DNA damage

The formation of oligo-nucleosomal DNA fragments were assessed using an electrophoretic technique called "DNA ladder" that reveals a visual profile of DNA damage. The results of DNA ladder experiments are presented in Fig. 6.10. It is evident from the profile that complexes **C1-C3** shows ladder like patterns indicating apoptosis due to fragmentation of the genomic DNA. Results reveal that metal complexation enhance the apoptotic effect of the fluoroquinolone drugs and curcumin in A-549 cells [12].

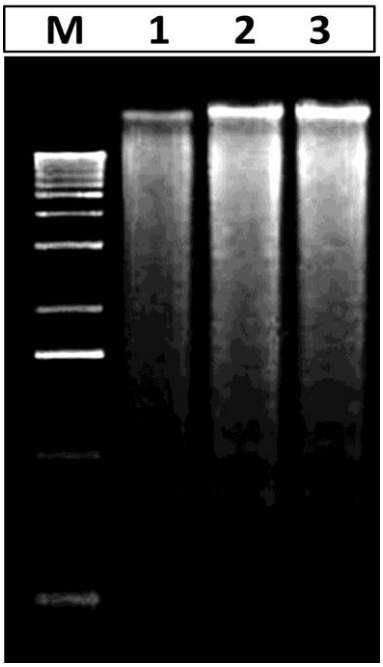

Fig 6.10: Photogenic view of cleavage of A-549 cells with **C1-C3** using 1.5% agarose gel containing ethidium bromide. All complexes were incubated for 16 h at 37 °C. Lane 1, Marker M; Lane 2, **C1**; Lane 3, **C2**; Lane 4, **C3.**

6.4.2.7 Western blot Analysis

Caspases are a family of cysteine proteases that play essential roles in apoptosis (programmed cell death).Caspases are known to mediate the apoptotic pathway [13, 14]. To clarify the mechanism of apoptosis induced by **C1-C3**, activation of caspases 3 and cleavage of PARP was assayed by Western blotting analysis. Results revealed that on treatment of A549 cells with **C1-C3,** the level of caspase 3 increases (activated caspases, Fig. 6.11). PARP, a 116-kDa nuclear poly (ADP-ribose) polymerase, appears to be involved in DNA repair, predominantly in response to environmental stress [15]. This protein can be cleaved by many interleukin-1β converting enzymes like caspases in vitro [16, 17] and is one of the main cleavage targets of caspase-3 in vivo [18, 19]. For human PARP, the cleavage occurs between Asp214 and Gly215, which separate PARP's N-terminal DNA binding domain (24 kDa) from its C-terminal catalytic domain (89 kDa) [16, 18]. PARP is important for cells to maintain their viability; cleavage of PARP facilitates cellular disassembly and serves as a marker of cells undergoing apoptosis [20,21]. The complexes were tested for Caspase 3 activation and PARP cleavage in A549 cells by incubating for 16 h and the cleavage pattern was analyzed by western blot. As depicted in Fig. 6.11 all the 3 complexes caused PARP cleavage through activation of caspase 3.

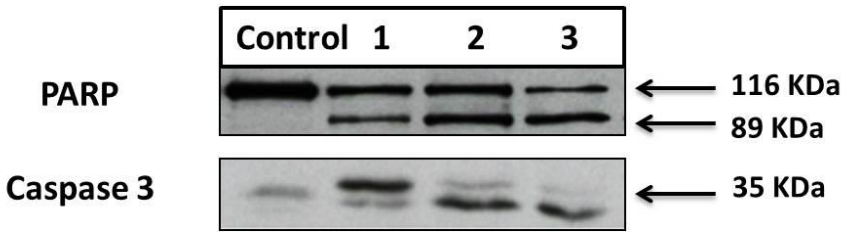

Fig 6.11: The cleavage of caspase-3 and PARP-1 proteins was evaluated in A549 cells, treated for 16 h with complexes **C1-C3**. The expression of GAPDH protein was employed as an internal loading control. Representative Western blots are shown. The experiments were repeated twice with comparable results.

6.5 Conclusion

The synthesis and characterization of **3** mixed ligand complexes of the third-generation fluoroquinolone antibacterial drug moxifloxacin (MFL) and curcumin (cur) with the metal ions Cu^{2+},VO^{2+},$^{+}$and Zn^{2+} has been achieved with physicochemical and spectroscopic methods. The design of the complexes was to stabilize the hydrolytically unstable curcumin, on binding to a metal (II) center which in turn was bound to MFL for better lipophilicity.

As determined by MTT assay, all the 3 complexes caused cellular growth inhibition in a concentration and time-dependent manner, with **C1** exhibiting highest cytotoxicity. Fluorescence microscopy revealed the cytosolic localization of the complexes **C1-C3** in A549 cancer cells. In addition, **C1-C3** enhances the level of intracellular ROS and induces a decrease of mitochondrial membrane potential. The cell cycle arrest studies demonstrated that the antiproliferative effect induced by **C1-C3** on A549 cells occured in G0/G1 phase of the cell cycle. Annexin-V /PI staining (FACS) of cells also indicated that the complexes induce cell death through the apoptotic pathway. Western blotting analysis showed that **C1-C3** activate caspase 3 and cleave PARP. Thus overall results indicated that the curcumin complexes induced apoptosis of A549 cells through mitochondrial dysfunction leading to release of cytochrome c and activation of caspases and cleavage of PARP. This whole process was ROS mediated. The results of our current studies provided strong experimental evidence for the use of mixed ligand curcumin metal complexes as therapeutic agents for treatment of lung cancer.

References

[1] B. B. Aggarwal, C. Sundaram, N. Malani and H. Ichikawa, Curcumin: The Indian Solid Gold, Springer, New York, 2001.

[2] G. P. Lim, T. Chu, F. Yang, W. Beech, S. A. Frautschy and G. M. Cole,J. Neurosci., 21 (2001) 8370.

[3] R. Waranyoupalin, S. Wongnawa, M. Wongnawa, C. Pakawatchai P. Panichayupakaranant and P. Sherdshoopongse, Cent. Eur. J. Chem., 7 (2009) 388.

[4] A. Goel, A. B. Kunnumakkara and B. B. Aggarwal, Biochem. Pharmacol., 75 (2009) 787.

[5] M. M. Yallapu, M. Jaggi and S. C. Chauhan, Drug Discovery Today., 7 (2012) 71.

[6] P. Anand, A. B. Kunnumakkara and B. B. Aggarwal, Mol. Pharmaceutics., 4 (2007) 807.

[7] S. Wanninger, V. Lorenz, A. Subhan and F. T. Edelmann , Chem. Soc. Rev., 44 (2015) 4986.

[8] A. Jemal, R. Siegel, E. Ward, T. Murray, J. Xu, C. Smigal, M.J. Thun, Cancer statistics, 2006, CA Cancer J. Clin. 56 (2006) 106.

[9] A. Cindy, Puckett, J.K. Barton, J. Am. Chem. Soc., 129 (2007) 46.

[10] C. Riccardi, I. Nicoletti, Nat. Protoc., 1 (2006) 1458.

[11] (a) E. Junn, K.N. Lee, H.R. Ju, I. Choi *et al*, J. Immunol., 165 (2000) 2190.
(b) N. Ames, M.K. Shigenaga, T.M. Hagen, Proc Natl Acad Sci USA., 90 (1993) 7915.

[12] R. Singh, R. N. Jadeja, M. C. Thounaojam, T. Patel, R.V. Devkar, D. Chakraborty, Inorganic Chemistry Communications, 23 (2012) 78.

[13] G.S. Salvesen, V.M. Dixit, Cell., 91(1997) 443.

[14] N.A. Thornberry, Y. Lazebnik, Science., 281(1998)1312.

[15] S. Cory, D.C, Huang, J.M. Adams, Oncogene., 22 (2003) 8590.

[16] M.S. Satoh, T. Lindahl, Nature., 356 (1992) 356.

[17] Y. Lazebnik, S. Kaufmann, S. Desnoyers, G. Poirier, W. Earnshaw, Nature., 371(1994) 346.

[18] G.M. Cohen, J. Biochem., 326(1997) 1.

[19] D.W. Nicholson, A. Ali, N.A. Thornberry, Y.A. Lazebnik *et al.* Nature., 376 (1995) 37.

[20] M. Tewari, L.T. Quan, K. O'Rourke, S. Desnoyers, Z.Zeng, D.R. Beidler, G.G. Poirier, G.S. Salvesen, V.M. Dixit, Cell., 81(1995) 801.

[21] F.J. Oliver, G. Rubia, V. Rolli, M.C. Ruiz-Ruiz, G. Murcia, J. Menissier-de Murcia, J. Biol Chem., 273 (1998) 33533.